Title: MDS-associated *SF3B1* mutations promote aberrant fate choice of hematopoietic stem cell via mis-splicing of mediator kinase module component CDK8

Elizabeth A. Bonner[1,2], Tun-Yun Hsueh[2], Axia Song[2], Erica A. Arriaga-Gomez[2], Rasika Venkataraman[2,3], Sayantani Sinha[2], Evan Nguyen[2], P. Brent Ferrell[4], Robert S. Welner[5], Rui Lu[5], Derek L. Stirewalt[2], Sergei Doulatov[6], Stanley C. Lee[2,7]

[1]Molecular and Cellular Biology Graduate Program, University of Washington, Seattle, WA, USA

[2]Translational Science and Therapeutics Division, Fred Hutchison Cancer Center, Seattle, WA, USA

[3]Molecular Medicine and Mechanisms of Disease Graduate Program, University of Washington, Seattle, WA, USA

[4]Department of Medicine, Division of Hematology/Oncology and Vanderbilt-Ingram Cancer Center, Vanderbilt University Medical Center, Nashville, Tennessee, USA

[5]Division of Hematology/Oncology and O'Neal Comprehensive Cancer Center at the University of Alabama at Birmingham, Birmingham, USA

[6]Department of Physiology and Cellular Biophysics, Columbia University, New York, USA

[7]Department of Laboratory Medicine and Pathology, University of Washington, Seattle, WA, USA

Running Title: SF3B1 mutations disrupt CDK8 function in MDS.

Corresponding author:
Stanley C. Lee, Ph.D.
Translational Science and Therapeutics Division
Fred Hutchinson Cancer Center
1100 Fairview Ave N.
Seattle, WA 98109, USA.
Email: sclee3@fredhutch.org
Phone: +1-206-667-1004

ABSTRACT

Mutations in the RNA splicing factor *SF3B1* are among the most common in MDS and are strongly associated with MDS with ring sideroblasts (MDS-RS). While aberrant splicing of terminal erythroid regulators has been implicated in MDS pathogenesis, the impact of *SF3B1* mutations on early hematopoietic progenitor function remains unclear. Here, we identify CDK8, a key kinase of the mediator complex involved in transcriptional regulation, as a recurrent mis-spliced target in *SF3B1*-mutant MDS. Mutant SF3B1 induces cryptic 3′ splice site selection in CDK8, leading to loss of CDK8 mRNA and protein. Using primary human HSPCs, our study identifies CDK8 as an important regulator of HSPC homeostasis and cell fate determination. CDK8 depletion results in expanded primitive HSPCs and shifts differentiation toward the and erythroid lineages, mirroring phenotypes observed in *SF3B1*-mutant MDS, and functional rescue of CDK8 rescues early erythroid phenotypes in *SF3B1*-mutant cells. These findings implicate CDK8 mis-splicing as a mechanistic driver of altered progenitor fate and dysplasia in SF3B1-mutant MDS, linking aberrant splicing to transcriptional dysregulation and hematopoietic lineage commitment.

INTRODUCTION

Myelodysplastic syndromes (MDS) are a heterogenous group of age-related clonal myeloid disorders characterized by cytopenia, morphologic dysplasia, and an increased risk of developing secondary acute myeloid leukemia (AML). The etiology of MDS can be broadly attributed to the complex interplay between genetic, epigenetic and environmental factors that cause functional abnormalities in bone marrow resident hematopoietic stem cells (HSCs), leading to clonal outgrowth and ineffective hematopoiesis. Somatic mutations in the RNA splicing factor *SF3B1* are highly prevalent in MDS, occurring in ~25% of patients, and in over 70% of patients with ring sideroblasts (MDS-RS).[1-6] SF3B1 is a member of the U2 small nuclear ribonucleoprotein (U2 snRNP) complex, which is responsible for intronic branchpoint recognition, an essential step in pre-mRNA splicing. MDS-associated *SF3B1* mutations occur in hot-spot regions within the heat domains, and confer neomorphic activity that commonly results in cryptic branchpoint selection and the preferential usage of intron-proximal 3' splice sites.[7-12] Aberrant splicing of transcripts such as ABCB7, TMEM14C, MAP3K7, EFRE and PPOX by mutant SF3B1 have been directly linked to impaired terminal erythroid maturation, deregulation of iron homeostasis and ring sideroblast formation, which are pathognomonic features of MDS-RS.[9, 13-16]

In addition to alterations in cellular splicing repertoires, RNA sequencing has demonstrated that *SF3B1* mutations cause alterations to the global transcriptional landscape of hematopoietic stem and progenitor cells (HSPCs). Single cell transcriptomic analysis of *SF3B1*-mutant $CD34^+$ HSPCs shows that the cell transcriptional states of mutant HSPCs largely accumulate in myeloid and erythroid progenitor compartments and may be primed for preferential differentiation along the erythroid lineage.[17, 18] While many individual mis-spliced targets have been linked to deficits in late erythroid development, how mutant *SF3B1* disrupts the function of early hematopoietic progenitors remains unclear. Because a vast body of evidence has shown that lineage

commitment is heavily reliant on appropriate gene expression to facilitate hematopoietic differentiation,[19-23] we hypothesize that *SF3B1* mutations may be disrupting transcriptional cofactors responsible for fine tuning gene expression.

In this study, we discovered that CDK8, a member of the mediator kinase module, is consistently mis-spliced in *SF3B1*-mutant MDS. CDK8 is the catalytic component of mediator kinase module, an accessory subunit of mediator complex that bridges transcription factors with the RNA polymerase II (RNAPII) machinery and integrates various cellular signals to modulate transcriptional output[24] . Initially thought to function as a transcriptional repressor through phosphorylation of the RNAPII C-terminal domain,[25, 26] published work indicates CDK8 functions as a transcriptional activator in the hypoxia response network and p53 pathways.[27, 28] Additionally, CDK8 kinase activity has shown to be an important modulator of various signaling pathways such WNT, TGFβ, and INFγ signal cascades by phosphorylating downstream effectors such as c-MYC, SMADs, STAT1 and STAT3.[29-36] Given the pleiotropic roles of CDK8 as a transcriptional regulator, we investigated how MDS-associated *SF3B1* mutations promote CDK8 deregulation and its impact on dysplastic hematopoietic differentiation in MDS.

RESULTS

Focused RNA-seq analysis of transcriptional cofactors identifies recurrent mis-splicing of CDK8 in *SF3B1*-mutant MDS patients.

To identify candidate transcriptional co-factors which undergo mutant SF3B1-mediated aberrant splicing, we performed splicing analysis[37] using RNA sequencing data from isogenic leukemia lines (K562 *SF3B1*-WT, K562 *SF3B1*-K700E, and HNT34, a leukemia cell line that harbors an endogenous *SF3B1*-K700E mutation), as well as publicly available MDS patient samples with and

without *SF3B1* mutations.[38, 39] We curated a list of 162 transcriptional co-factors using gene ontology[40, 41] (**Supplimental Table S1**) and looked for significant splicing events from our cohort that followed a set of criteria: 1) The splicing event must be enriched in *SF3B1* mutant cells compared to wild-type (WT), 2) the splicing event deregulates transcript stability, 3) mis-splicing must occur across different SF3B1 mutations, 4) the splicing event is exclusive to *SF3B1* mutations. Using a delta percent spliced-in (dPSI) cut off of 0.08 and FDR <0.05, our analysis showed that, of the transcripts predicted to undergo alternative 3' splice site usage, members of the mediator complex are highly enriched, including MED13L, MED6 and CDK8 (**Figure 1A**). Because alternative splice site usage can lead to either stable alternative isoform usage or can introduce a premature termination codon, we next asked if any of the transcriptional co-factors also displayed changes in transcript level by RNA sequencing (**Figure 1B**). We performed differential gene expression analysis using DESeq2[42] and found that, among the 20 predicted mis-splicing events, only three transcripts (CDK8, TAF6L, TAF2) showed significant changes in expression (adjusted p-value <0.05). Notably, CDK8 was the only mediator complex member with significantly altered transcript levels. To determine if changes in CDK8 mRNA levels were specific to the *SF3B1*-K700E mutation, we performed differential expression analysis on a larger cohort of MDS patients with and without *SF3B1* mutations,[38, 43-45] healthy bone marrow and *SF3B1*-WT (K562) and *SF3B1*-K700E (K562, HNT34) cell lines (**Figure 1C**). While TAF6L displayed a greater decrease in mRNA expression in *SF3B1*-mutant samples, alternative 3' splice site usage in both patient samples and cell lines is significantly enriched in the *SF3B1*-WT cells (**Figure 1A, Supplimental Figure S1A),** which did not meet our criteria. Similarly, the mis-splicing of MED13L, TAF2, and MED6 in *SF3B1*-mutant cells did not meet our criteria, either due to a lack of significant transcript downregulation or because the resulting splice variants generated stable mRNA isoforms (**Supplimental Figure S1B-H)**.

Due to alternative 3′ splice site usage, CDK8 is predicted to include 14-base pairs of intronic sequence proximal to exon 8. To confirm this, we examined CDK8 read coverage in the Integrated Genome Viewer[46] (IGV) and observed intronic inclusion exclusively in samples from *SF3B1*-mutant cells (**Figure 1D**). Additionally, we did not observe CDK8 mis-splicing in other common spliceosome mutations (**Supplimental Figure S1I)** Taken together, these data indicate that *SF3B1* mutations affect only a small subset of transcriptional co-factors, and among those, CDK8 is the only one consistently showing decreased mRNA transcript levels across different *SF3B1*-mutant contexts. (**Supplimental Figure S1A-D**)

Mutant SF3B1-induced mis-splicing of CDK8 results in loss of expression via nonsense-mediated decay

We next sought to validate CDK8 mis-splicing in *SF3B1*-mutant MDS patient samples and cells lines. We designed PCR primers which spanned exon-exon boundaries around CDK8 exon 8 and performed RT-PCR followed by native polyacrylamide gel electrophoresis (PAGE). We could detect the 14 base-pair intronic sequence inclusion in *SF3B1*-mutant but not *SF3B1*-WT isogenic cell lines (**Figure 1E**). We then wanted to determine if reductions in CDK8 mRNA corresponded to a reduction of CDK8 at the protein level. We performed western blot in *SF3B1*-mutant cell lines and found that CDK8 protein was reduced in SF3B1 mutant samples but not their WT counterparts (**Figure 1F**). The inclusion of 14 base pairs of intronic sequence is predicted to lead to a frame shift, leading to reduction of CDK8 mRNA by the quality surveillance pathway nonsense-mediated decay (NMD). To verify this prediction, we treated cells with a NMD inhibitor, NMDi-14, and performed qPCR in isogenic *SF3B1*-mutant cell lines. We found that NMDi-14 treatment restored CDK8 mRNA levels in *SF3B1*-mutant cells but not in *SF3B1*-WT cells (**Figure 1G**). Together, these data verify that CDK8 is mis-spliced by mutant SF3B1 leading to reduction of CDK8 mRNA and protein due to mRNA degradation by NMD.

Loss of CDK8 causes defective hematopoietic stem and progenitor cell function and muti-lineage differentiation *in vitro* and *in vivo*

Phenotypically, *SF3B1*-mutant MDS patients present with an expansion of erythroblasts and single cell transcriptomic data has indicated that *SF3B1*-mutant HSPCs have an accumulation of cell states resembling early erythroid and myeloid precursors.[13, 17, 18, 47, 48] To determine if CDK8 loss is contributing to the shift in frequency of early myeloid and erythroid progenitors, we used a dual-guide RNA-based CRISPR/Cas9 system[49] to target CDK8 ($CDK8^{KO}$) or the AAVS1 (NTC) locus as a negative control in human $CD34^+$ HSPCs (**Supplimental Figure S2A-C**). To monitor differentiation along a single lineage, we used GCSF-mobilized healthy adult $CD34^+$ cells and performed liquid culture differentiation along the myeloid or erythroid axis. We found that $CDK8^{KO}$ HSPCs produced a higher percentage of $CD13^+CD14^+$ myeloid cells, and $CD71^+CD235a^+$ erythroid cells compared to NTC cells (**Figure 2A-B**). To monitor multi-lineage differentiation of early progenitors, we generated $CDK8^{KO}$ cells from umbilical cord blood-derived $CD34^+$ HSPCs (UCB) and performed colony-forming unit (CFU) assays (**Figure 2C**). Our data showed that $CDK8^{KO}$ HSPCs generated significantly more colonies, driven by a marked increase in CFU-Granulocyte/Macrophage (CFU-G/M) colonies. While CDK8 knock did not produce a significant increase in the number of early burst-forming erythroid colonies (BFU-E), we found that when we collected total colonies at the end of the experiment, $CDK8^{KO}$ colonies produced much redder pellets (**Figure 2D**). Together, these results indicate that CDK8 loss leads to increased differentiation along the myeloid and erythroid axes and supports our hypothesis that CDK8 mis-splicing may be contributing to the expansion of early erythroid and myeloid progenitors in *SF3B1*-mutant MDS.

To determine the long-term *in vivo* consequences of CDK8 loss in hematopoiesis, we used the same CRISPR/Cas9 system to knockout CDK8 in UCB $CD34^+$ cells followed by xenotransplantation in NOD/SCID/ILR2γ-null (NGS) mice (**Supplimental Figure S3A**). At terminus (20 weeks post xenotransplantation), we harvested spleen, bone marrow and peripheral blood to assess lineage composition and confirm knock-down in bone marrow $CD45^+$ cells (**Supplimental Figure S2C-D**). $CDK8^{KO}$ UCB mice had a mild increase in $CD33^+$ myeloid cells in the blood and bone marrow (**Supplemental Fig. S3C-E**). There were no significant differences between the level of human cell chimerism (%$CD45^+$) in the bone marrow mononuclear cell fraction of mice transplanted with $AAVS1^{KO}$ or $CDK8^{KO}$ HSPCs (**Supplimental Figure S3F**). Interestingly, we observed a significant increase $CD14^+CD16^+$ intermediate monocytes in the bone marrow (**Figure 2E**). Further examination of the bone marrow HSPC fraction (defined by $CD45^+lineage^-CD34^+$) revealed there was no significant increase in the total number of HSPCs between $AAVS1^{KO}$ and $CDK8^{KO}$ groups (**Figure 2F**). Interestingly, we observed a mild but significant increase in the proportions of the more immature progenitors (defined by $CD45^+lineage^-CD34^+CD38^-$) and lymphoid-primed multipotent progenitors (LMPP, defined by $CD45^+lineage^-CD34^+CD38^-CD45RA^+CD90^-$) (**Figure 2G-H, Supplimental Figure S3G**). When we looked within the more differentiated myeloid progenitor fraction (defined by $CD45^+lineage^-CD34^+CD38^+$), we observed a significant decrease in classically defined immunophenotypic megakaryocyte-erythroid progenitors (MEPs; $CD45^+lineage^-CD34^+CD38^+CD45RA^-CD123^-$) and granulocyte-macrophage progenitors (GMPs; $CD45^+lineage^-CD34^+CD38^+CD45RA^+CD123^+$) (**Figure 2I)**. While we do not see an expansion in immunophenotypic MEPs or GMPs, we observed a significant expansion in a distinct subset of cells within the $CD34^+CD38^+$ compartment that express CD71 (**Figure 2J**), a population with the potential to differentiate into both erythroid and granulocytic lineages.[50, 51] Our *in vivo* data indicates that loss of CDK8 leads to an expansion of specific primitive HSPC compartments that skew towards the erythroid and granulocytic/myeloid differentiation trajectories.

CDK8-deficient loss deregulates homeostatic- and lineage-specific transcriptional pathways in HSPCs

Because CDK8 functions as transcriptional modulator, we next sought to determine the changes resulting from CDK8 loss in UBC $CD34^+$ HSPCs. We performed RNA sequencing in $CD34^+$ UCB cells treated with 2 independent short-hairpin RNAs (shRNAs) targeting CDK8 (shCDK8) or a non-targeting control (shNTC) (**Figure 3A, Supplimental Figure S4A-C**). We performed differential expression analysis (DESeq2) and filtered for significant (padj <0.05) changes shared across both hairpins (**Figure 3B,** solid dots). We found that CDK8-deficient $CD34^+$ cells had increased expression of known markers of myeloid differentiation (CD14, CECAM6, S100A8, S100A9), and decreased expression in signaling intermediates of key intracellular signaling pathways including the MAP kinase signaling (FOS, FOSB, JUN, DUSP2), JAK/STAT pathway (SOCS3) and GPCR signaling (RGS1, RGS2) pathways (**Figure 3A, Supplimental Figure S4D**). We then asked if we could detect similar patterns of deregulation in our MDS patient cohort. We found that most of the transcripts deregulated in CDK8-deficient $CD34^+$ HSPCs showed a similar expression pattern in *SF3B1*-mutant MDS patients (**Figure 3C**). Taken together, these results indicate that CDK8 loss is leading to deregulation of several important transcriptional networks, likely resulting in the upregulation of genes associated with lineage differentiation.

Restoration of CDK8 partially rescues erythroid differentiation defects in *SF3B1*-mutant iPSC model

Next, we sought to formally demonstrate the causal link between the phenotypic consequences of CDK8 loss to *SF3B1* mutations in MDS. To address this, we used a previously established isogenic pair of induced pluripotent stem cell-derived hematopoietic progenitor cell lines (iPSC-

HPCs) generated from an MDS-RS patients with an *SF3B1*-G742D mutation[52] (Supplimental **Figure S5A**). We also observed in the iPSC-HPC model that CDK8 is robustly mis-spliced and downregulated at both the mRNA and protein level in *SF3B1*-mutant cells relative to their *SF3B1*-WT isogenic counterparts (**Figure 4B-C, Supplimental Figure S5B**). Consistent with prior erythroid differentiation data, we observed that *SF3B1*-mutant iPSC-HPCs have a sharp increase in early erythroid cells ($CD71^{+}CD235a^{-}$). We therefore hypothesized that this early expansion of erythroid progenitors may be due to loss of CDK8. To determine if restoration of CDK8 could rescue erythroid differentiation defects in *SF3B1*-mutant cells, we stably introduced CDK8 cDNA or an empty vector (EV) control in *SF3B1*-mutant iPSC-HPCs and performed erythroid differentiation (**Figure 4A & 4D**). Compared to EV-transduced *SF3B1*-mutant cells, re-expression of CDK8 significantly reduced the expansion of $CD71^{+}CD235a^{-}$ cells (**Figure 4E & 4G**). Surprisingly, as differentiation continued, re-expression of CDK8 in this model continued to repress expansion of erythroid cells (**Figure 4F & 4H**). Taken together, our data indicates that the aberrant erythroid expansion and differentiation phenotype characteristic of *SF3B1* mutations in MDS-RS is partly mediated through mis-splicing and the subsequent loss of CDK8 function.

DISCUSSION

SF3B1 mutations are purported as functional drivers of expansion in clonal hematopoiesis and MDS. However, despite extensive research, the mechanistic understanding of how splicing defects confer a competitive advantage and skew early HSPC cell fate choice remain elusive. Here, we have utilized publicly available patient transcriptomics data,[38, 43-45] *ex vivo* and *in vivo* models to identify CDK8 mis-splicing as a potential mechanism governing impaired hematopoiesis. Our findings highlight CDK8 as a critical effector in *SF3B1*-mutated MDS and elucidated its importance in regulating proper hematopoietic differentiation.

SF3B1 is one of the most commonly mutated genes and the most frequently mutated spliceosome component in MDS and is associated with widespread splicing deregulation.[1-6, 8-12, 43, 53-56] Here, we identify CDK8 as a recurrent mis-splicing target in *SF3B1*-mutant MDS patients across a range of hotspot mutations. Mis-splicing led to deregulation of CDK8 transcript levels in mutant cells due to the introduction of a premature termination codon, resulting in CDK8 degradation by the quality surveillance pathway nonsense mediated decay.

Previous studies have linked *SF3B1* mutations to impaired terminal erythroid differentiation, iron metabolism and the formation of ring sideroblasts,[13, 16, 43, 54] but a mechanistic link between clonal advantage and early fate choice of HSPCs had not been made. Here, we show that, as a result of CDK8 loss, primitive HSPCs compartments expand *in vivo* and may preferentially differentiate along the myeloid and erythroid axes *in vitro* and *in vivo*. This skewed differentiation parallels the expansion of immature erythroid and myeloid precursors observed in *SF3B1*-mutant MDS patients and from *SF3B1*-mutant HSPCs from single cell transcriptomic studies. Thus, our findings provide a mechanistic link between *SF3B1* mutations and disrupted early HPSC fate via impaired CDK8-mediated transcriptional control.

CDK8 is well known as a context-specific transcriptional regulator in solid tumors, influencing pathways like WNT, p53 and STAT signaling.[29-36] Using RNA sequencing, our study identifies CDK8 as an important regulator of myeloid marker gene expression and indicates that deregulation of MYC and STAT pathways may be driving altered HSPC cell fate choice in *SF3B1*-mutant cells. Further supporting our findings, published work has shown that both MYC and JAK/STAT pathways play important regulatory roles in HSPC self-renewal, lineage commitment, and leukemogenic transformation.[57-63]

SF3B1-mutant MDS is generally considered low-risk, with current treatments focused on managing anemia. Our Data shows that reintroduction of CDK8 rescues erythroid abnormalities in *SF3B1*-mutant cell models and suggests a targeted approach to correcting differentiation defects, potentially through the use of splice correcting antisense oligonucleotides (ASOs), may be a therapeutic viability. Additionally, the observation that CDK8 loss enhances erythroid output underscores its therapeutic relevance, particularly given the abundance of available CDK8 kinase inhibitors that could be repurposed to promote erythropoiesis in other anemic conditions.

ACKNOWLEDGEMENTS

We thank Sean Bennette for counsel on bioinformatics, Anthony Rongvaux and Stefan Radtke on experiments involving immunocompromised mice, Beverly Torok-Storb for her mentorship, Daniel Kuppers for advice on gene editing, Laura Baquerro-Galves for advice on iPSC-HPC culture, and the Subramanaian and Tapscott labs at Fred Hutch for equipment loan. We would like to also acknowledge the Fred Hutch Cancer Center/University of Washington Hematopoietic Diseases Repository (FHCC/UW-HDR) for the use of primary MDS specimen, and the Fred Hutch Flow Cytometry, Genomics, and Comparative Medicine Shared Resources. R. Venkataraman is supported by the American Society of Hematology Graduate Hematology Award; S. Sinha is supported by the American Cancer Society Postdoctoral Fellowship; R.L. is supported by grants from the Mark Foundation for Cancer Research Endeavor Award, NIH/NCI (R01CA259480), American Cancer Society (RSG-22-036-01-DMC), and the Gabrielle's Angel Foundation for Cancer Research; S.C. Lee is supported by grants from the Edward P. Evans Foundation Discovery Research Grant, the American Society of Hematology Scholar Award and Bridge Grant, the Mark Foundation for Cancer Research Endeavor Award, the National Institute of Diabetes and Digestive and Kidney Diseases (RC2DK127989) and the National Cancer Institute

(R01CA292932). This research is also supported by the Fred Hutchinson Cancer Center Shared Resources through NCI Cancer Center Support grants (P30CA015704 and S10OD028685).

METHODS

Antibodies and oligos

All antibody information is available in **Supplementary Table S2**. All primers used in this study are available in **Supplimental Tables S3** respectively.

Cell Culture

Human umbilical cord blood CD34$^+$ cells (STEMCELL Technologies) and GCSF-mobilized adult CD34$^+$ cells (Fred Hutch Co-Operative Center for Excellence on Hematology (CCEH)) were thawed according to the manufacturer's instructions. Cells were cultured in SFEM-II (STEMCELL Technologies) supplemented with recombinant human cytokines (50 ng/mL SCF, 50 ng/mL FLT3L, 50 ng/mL TPO; all from Peprotech), 10 µg/mL LDL (STEMCELL Technologies), 500 nM SR1 (Selleck Chem.), 1 µM UM729 (STEMCELL Technologies) for 24 hours prior to nucleofection. K562, 293T, HNT34, and Nalm6 cells were cultured in base media (IMDM, DMEM, and RPMI, respectively) supplemented with penicillin-streptomycin (100 U/mL, Gibco, No. 15140122), Glutamax (1%, Gibco, No. 35050061) and heat-inactivated FBS (10%: K562, 293T, NALM6, 20%: HNT34). The MDS-RS patient derived *SF3B1*-G742D and isogenic *SF3B1*-WT iPSC-derived hematopoietic progenitors (iPSC-HPCs) were generated and maintained as previously described.[64] Briefly, cells were maintained in SFEM-II (STEMCELL Technologies) supplemented with penicillin-streptomycin (100 U/mL, Gibco, No. 15140122), doxycycline (2 µg/mL) and cytokines (10 ng/mL IL-3, 50 ng/mL IL-6, 50 ng/mL TPO, 50 ng/mL SCF, 50 ng/mL

FLT3L). Cells were washed and replated at a density of 5-7x10^5 cells/ mL every 3 days and not allowed to exceed 1.5x10^6 cells/mL. The iPSC-HPCs were maintained in culture for no more than 7 weeks. All cell lines were maintained in a 37°C/5% CO_2 incubator.

Gene Editing

Nucleofection of $CD34^+$ HSPCs was carried out as previously described [65] using the P3 4D Nucleofector kit (Lonza). Briefly, 24 hours post-thaw, 2-4 x10^5 cells were collected and rinsed in PBS and re-suspended in 20 μL nucleofection media consisting of 2.5 pmol/μL Sp.Cas9 (Aldeveron), 2.5 pmol/μL guide RNA (1.25 pmol/μl each guide, Synthego), in nucleofector solution supplemented with buffer P3. Cells were nucleofected in the 4D nucleofector (Lonza) using program DS 150 for buffer P3. Cells were recovered in 200 μL complete SFEM-II (see above) and allowed to recover for 24 hours prior to use. For applications requires greater cell numbers, multiple nucleofection reactions were performed and subsequently mixed post nucleofection. Guides in **Supplimental Table S3**.

Lentivirus production

Lentiviral particle production was performed using low-passage 293T cells (Takara ClonTech). Cells were seeded in 10 cm tissue culture dishes at a density of 3.2x10^4 cells/cm^2 in 10 mL complete DMEM (see above). 2 hours prior to transfection media was removed and replaced with 8 mL complete DMEM (see above). Transfection was performed 24 hours post plating by adding transfection master mix. To make the transfection master mix 12 μg of viral plasmid, and 12 μg of packaging viral mix (3:1 ratio of psPAX2:VSVG) was added to 2.34 mL Optimem (Gibco). 30 μg of polyethylenimine (Polysciences, 23966-100) was added to the media/plasmid solution and

vortexed for 30 seconds. Transfection master mix was allowed to sit at room temperature for 20 minutes prior to adding it to 293T cells, drop-wise. Complete media changed was performed 16 hours post-transfection by removing media/transfection mix and replaced with 10.5 mL of complete DMEM. Supernatants containing lentiviral particles were harvested 72 hours post transfection, snap-frozen in liquid nitrogen, and stored at -80ºC. To concentrate lentiviral particles, fresh viral supernatant was first filtered of cell debris in using Millex -GP syringe filters (Millipore, SLGVM33RS), and concentrated using Amicron Ultra-15 centrifugal filter units (Millipore, UFC905024), snap frozen and stored at -80ºC

Immunoblotting

Cells were lysed in RIPA buffer (Invitrogen, CAT#89900) supplemented with protease inhibitors (ThermoFisher, CAT#78446) and sonicated (Bioruptor UCD-200, Diagenode) for 5 minutes in 30 second on/off cycles on medium setting. Protein concentrations were normalized using a Pierce BCA protein assay kit (Thermo Fisher Scientific CAT#23227). 20 ng of protean lysate was mixed with 6XSDS loading buffer (0.3M Tris-HCL, 10% SDS, 60% Glycerol, 6% 2-mercaptoethanol, 1% bromophenol blue), loaded in pre-cast SDS acrylamide gels (BioRad, CAT#4561084) and run at 90V. Blots were transferred using the Bio-Rad turbo transfer apparatus following manufacturers recommendation. Membranes were blocked in Tris-buffered saline with 0.05% Tween-20 (TBS-T) and 5% milk for 1h at room temperature and immunoblotted with primary antibodies overnight at 4°C. Antibodies are listed in **Supplimental Table S2**. Membranes were washed 3 times with TBS-T and incubated for 1 h at room temperature with secondary antibodies conjugated to horseradish peroxidase. Blots were imaged using ECL Substrate (BioRad, CAT#1705062) using AFP mini-medical 90 film processor.

RT-PCR

200 ng Trizol extracted RNA was used to make cDNA using iScript (BioRad, CAT# 1708891). PCR was performed using GoTAQ (Promega, CAT#M7123). PCR products were run using the Protean II xi electrophoresis tank (BioRad) in a 12% native polyacrylamide gel (BioRad, CAT#1610156) in 1XTBE (Fisher Chemical, SO-0016) at 45V for 48 hours at 4°C and imaged using ethidium bromide (Fisher Scientific, CAT#BP1302-10) on a Gel Doc XR (Bio-Rad). Primers are listed in **Supplimental Table S3.**

Flow Cytometry

Cells were harvested and washed in cold FACS buffer (1XPBS, 2%FBS). Cells were resuspended in 100 µL staining buffer (FACs buffer with a 1:200 dilution of each antibody) and incubated in the dark at 4C for 20 minutes. Staining buffer was washed by adding 1 mL FACS and resuspended in 100-300 µL FACS buffer with 1:500 dilution dapi (Millipore, 10236276001). Flow cytometry was performed on the BD FACSymphony A5. Antibodies are listed in **Supplimental Table S2**.

Animals

All animal experiments were performed with approval by and in accordance with Fred Hutchinson Cancer Center (FHCC) Institutional Animal Care and Use Committees guidelines. Animal experiments were performed within the FHCC Comparative Medicine facility. For xenotransplantation experiments, 6–7-week-old female NOD.Cg-*Prdkc*^{SCID} *Il2r*$\gamma^{-/-}$ (NSG) mice (Fred Hutch Comparative Medicine Shared Resources) were used. NSG mice were sub-lethally irradiated (2.0 cGy) 24 hours prior to transplantation. Twenty-four hours post recovery from nucleofection, ~4-8 x10^4 cells were transplanted intravenously via tail vein injection. Peripheral

blood was monitored by flow cytometry every 4 weeks to track human cell chimerism. At 20 weeks post-xenotransplantation, hematopoietic organs (bone marrow, spleen and peripheral blood) were harvested and analyzed by flow cytometry using antibodies against CD45, CD34, CD38, CD33, CD19, and CD3.

Ex vivo differentiation assays

For colony-forming unit (CFU) assays, umbilical cord blood-derived $CD34^+$ HSPCs were plated 24 hours post nucleofection in 1 mL MethoCult H4034 (STEMCELL Technologies). Cells were plated at a density of 500 cells/mL in triplicate plates. Colonies were counted and scored 11 days post-plating. For myeloid differentiation assays, healthy adult $CD34^+$ HSPCs were electroporated and plated at a density of 2.5 $x10^4$ cells/well in 96-well U-bottom plates in SFEM-II containing Myeloid II Expansion supplement (STEMCELL Technologies). Differentiation was monitored by flow cytometry for expression of CD14 and CD13. Erythroid differentiation was performed using healthy adult CD34+ HSPCs following previously described protocols.[66] Briefly, $1x10^5$ cells were plated in 1 mL of expansion media (SFEM supplemented with 100 ng/mL FLT3 ligand, 100ng/mL SCF, 5 ng/mL IL-3, 20 ng/mL IL-6) for 3 days. On day 4 cells were plated at a density of 1 $x10^5$ cells/ mL in Stage 1 media (IMDM, 15% FBS, 2 mM glutamine, 1% BSA, 500 µg/mL holo-transferrin, 10 µg/mL insulin, 100 ng/mL SCF, 5 ng/mL IL3, 6 U/mL EPO) and cultured for 5 days. On day 9 cells were plated at a density of $2x10^5$ cells/ mL in Stage 2 media (IMDM, 15% FBS, 2 mM glutamine, 1% BSA, 500 µg/mL holo-transferrin, 10 µg/mL insulin, 100 ng/mL SCF, 6 U/mL EPO). On day 14 cells were seeded at 3 $x10^5$ cells/mL in Stage 3 media (IMDM, 15% FBS, 2 mM glutamine, 1% BSA, 500 µg/mL holo-transferrin, 10 µg/mL insulin, 2 U/mL EPO). The appropriate media was supplemented in the middle of each stage to maintain cells at a density below 2 $x10^6$ cells/mL. Differentiation was monitored by flow cytometry for expression of CD71 and CD235a

RNA Sequencing

For cultured cell lines total RNA was isolated from 5 x10^6 K562 SF3B1^{WT}, K562 SF3B1^{K700E} or HNT34 cells using TRIzol according to the manufacturer's instruction. For CDK8 knock-down UCB derived CD34$^+$ cells, 0.2-3 x10^6 CD34$^+$ GFP$^+$ cells were sorted using the Symphony S6 sorter (BD Biosciences), followed by RNA isolation by Trizol. RNA quality was determined using Agilent RNA 6000 Nano chip on the Agilent 4200 TapeStation and quantification was performed using NanoDrop spectrophotometer (Thermo Fisher Scientific). Total RNA samples with RNA integrity number (RIN) >8 was selected for Illumina sequencing library preparation. One microgram of DNA-free total RNA was used to prepare the library using Ultra II Directional RNA Library Prep Kit (New England Biolabs, No. E7760L) following manufacturer's instructions. Paired end sequencing (150 bp) of the libraries were performed using an Illumina NovaSeq SP platform.

Amplicon Sequencing

Human CD45$^+$ cells were isolated from murine bone marrow 20 weeks post-transplant using the using the BD Symphony S6 sorter (BD Biosciences). DNA was extracted using the Qiagen DNeasy blood and tissue kit (CAT#69504). PCR was performed using Platinum II host start PCR master mix (Invitrogen, CAT#14000013). PCR products were precipitated overnight using ethanol precipitation (https://projects.iq.harvard.edu/files/hlalab/files/ethanol-precipitation-of-rna_hla.pdf) and submitted for sequencing at Azetna following submission guidelines.

Bioinformatic Analysis

For RNA sequencing, raw fastq files were trimmed and quality was assessed using TrimGalore (https://github.com/FelixKrueger/TrimGalore). Trimmed fastq files were aligned (GRCh38, Gencode Release 48) with STAR[67] using –quantMode GeneCounts. For publicly available MDS patient data batch correction was performed using limma[68] and differential expression for all datasets was performed using DESeq2[69] comparing wild type to mutant samples. Significant changes were determined using a cutoff of |Log2 fold change| $\geq$ 0.5 and p-adjusted value $\leq$ 0.05. For splicing analysis reads were aligned (GRCh38, Gencode Release 48) using STAR along with soft-clipping and splicing changes were quantified using rMATS-Turbo 4.1.1[70] with the novel splice site detection feature enabled.

To generate heat map plots of publicly available data, .JC files were imported using maser (https://github.com/DiogoVeiga/maser) and significant splicing events were determined (minimum read count =10, |PSI|$\geq$ 0.05, FDR <0.05). A list of 162 transcriptional cofactors was curated from gene ontology (https://geneontology.org/) and filtered for unique entries. Significant splicing events were filtered using the unique transcriptional cofactor list. Z scores were calculated for splicing events within each data set to control for batch effects and unsupervised clustering was performed across all samples within each splice type.

For amplicon sequencing analysis, quality and trimming was performed on raw fastq files (see above). Reads were aligned to CDK8 reference sequence (NCBI NC_000013.11) and analyzed using CRISPResso[71] using a window of 50 nucleotides surrounding the guide.

References

1. Malcovati, L., et al., *Clinical significance of SF3B1 mutations in myelodysplastic syndromes and myelodysplastic/myeloproliferative neoplasms.* Blood, 2011. **118**(24): p. 6239-6246.
2. Patnaik, M.M., et al., *SF3B1 mutations are prevalent in myelodysplastic syndromes with ring sideroblasts but do not hold independent prognostic value.* Blood, 2011. **119**(2): p. 569-569.
3. Papaemmanuil, E., et al., *Somatic SF3B1 Mutation in Myelodysplasia with Ring Sideroblasts.* The New England journal of medicine, 2011. **365**(15): p. 1384-1384.
4. Visconte, V., et al., *SF3B1, a splicing factor is frequently mutated in refractory anemia with ring sideroblasts.* Leukemia, 2012. **26**(3): p. 542-545.
5. Yoshida, K., et al., *Frequent pathway mutations of splicing machinery in myelodysplasia.* Chang Gung Memorial Hospital, 2011. **105**.
6. Haferlach, T., et al., *Landscape of genetic lesions in 944 patients with myelodysplastic syndromes.* Leukemia, 2014. **28**(2): p. 241-247.
7. Alsafadi, S., et al., *Cancer-associated SF3B1 mutations affect alternative splicing by promoting alternative branchpoint usage.* Nature Communications, 2016. **7**(1): p. 1-12.
8. Darman, Rachel B., et al., *Cancer-Associated SF3B1 Hotspot Mutations Induce Cryptic 3′ Splice Site Selection through Use of a Different Branch Point.* Cell Reports, 2015. **13**(5): p. 1033-1045.
9. Dolatshad, H., et al., *Disruption of SF3B1 results in deregulated expression and splicing of key genes and pathways in myelodysplastic syndrome hematopoietic stem and progenitor cells.* Leukemia, 2015. **29**(5): p. 1092-1103.
10. Inoue, D., et al., *Spliceosomal disruption of the non-canonical BAF complex in cancer.* Nature, 2019. **574**(7778): p. 432-436.
11. Kesarwani, A.K., et al., *Cancer-associated SF3B1 mutants recognize otherwise inaccessible cryptic 3′ splice sites within RNA secondary structures.* Oncogene, 2017. **36**(8): p. 1123-1133.
12. Seiler, M., et al., *Somatic Mutational Landscape of Splicing Factor Genes and Their Functional Consequences across 33 Cancer Types.* Cell Reports, 2018. **23**(1): p. 282-296.e4.
13. Clough, C.A., et al., *Coordinated missplicing of TMEM14C and ABCB7 causes ring sideroblast formation in SF3B1-mutant myelodysplastic syndrome.* Blood, 2022. **139**(13): p. 2038-2049.
14. H, D., et al., *Cryptic splicing events in the iron transporter ABCB7 and other key target genes in SF3B1-mutant myelodysplastic syndromes.* Leukemia, 2016. **30**(12): p. 2322-2331.
15. S, B., et al., *A variant erythroferrone disrupts iron homeostasis in SF3B1-mutated myelodysplastic syndrome - PubMed.* Science translational medicine, 07/10/2019. **11**(500).
16. Lieu, Y.K., et al., *SF3B1 mutant-induced missplicing of MAP3K7 causes anemia in myelodysplastic syndromes.* Proceedings of the National Academy of Sciences, 2021-12-20. **119**(1).
17. Benbarche, S., et al., *GPATCH8 modulates mutant SF3B1 mis-splicing and pathogenicity in hematologic malignancies.* Molecular Cell, 2024. **84**(10): p. 1886-1903.e10.
18. Cortés-López, M., et al., *Single-cell multi-omics defines the cell-type-specific impact of splicing aberrations in human hematopoietic clonal outgrowths.* Cell Stem Cell, 2023/09/07. **30**(9).

19. Antoniani, C., O. Romano, and A. Miccio, *Concise Review: Epigenetic Regulation of Hematopoiesis: Biological Insights and Therapeutic Applications.* STEM CELLS Translational Medicine, 2017/12/01. **6**(12).
20. Godini, R., J. Yan, and M. Chopin, *Frontiers | Transcriptional regulatory logic orchestrating lymphoid and myeloid cell fate decisions.* Frontiers in Immunology, 2025/05/29. **16**.
21. Göttgens, B., *Regulatory network control of blood stem cells.* Blood, 2015/04/23. **125**(17).
22. M, L. and P. R, *Global genetic regulatory networks controlling hematopoietic cell fates - PubMed.* Current opinion in hematology, 2006 Jul. **13**(4).
23. P, L., et al., *Gene regulatory networks directing myeloid and lymphoid cell fates within the immune system - PubMed.* Seminars in immunology, 2008 Aug. **20**(4).
24. Richter, W.F., et al., *The Mediator complex as a master regulator of transcription by RNA polymerase II.* Nature Reviews Molecular Cell Biology 2022 23:11, 2022-06-20. **23**(11).
25. H, E., et al., *The cyclin-dependent kinase 8 module sterically blocks Mediator interactions with RNA polymerase II - PubMed.* Proceedings of the National Academy of Sciences of the United States of America, 10/24/2006. **103**(43).
26. Knuesel, M.T., et al., *The Human CDK8 Subcomplex Is a Histone Kinase That Requires Med12 for Activity and Can Function Independently of Mediator.* Molecular and Cellular Biology, 2009. **29**(3): p. 650-661.
27. Galbraith, M.D., et al., *HIF1A Employs CDK8-Mediator to Stimulate RNAPII Elongation in Response to Hypoxia.* Cell, 2013. **153**(6): p. 1327-1339.
28. Donner, A.J., et al., *CDK8 Is a Stimulus-Specific Positive Coregulator of p53 Target Genes.* Molecular Cell, 2007. **27**(1): p. 121-133.
29. Firestein, R., et al., *CDK8 is a colorectal cancer oncogene that regulates β-catenin activity.* Nature 2008 455:7212, 2008-09-14. **455**(7212).
30. Morris, E.J., et al., *E2F1 represses β-catenin transcription and is antagonized by both pRB and CDK8.* Nature 2008 455:7212, 2008-09-14. **455**(7212).
31. Bancerek, J., et al., *CDK8 Kinase Phosphorylates Transcription Factor STAT1 to Selectively Regulate the Interferon Response.* Immunity, 2013. **38**(2): p. 250-262.
32. J, M.-F., et al., *CDK8 Fine-Tunes IL-6 Transcriptional Activities by Limiting STAT3 Resident Time at the Gene Loci.* Cell reports, 2020. **33**(12).
33. Johannessen, L., et al., *Small-molecule studies identify CDK8 as a regulator of IL-10 in myeloid cells.* Nature chemical biology, 2017. **13**(10): p. 1102-1102.
34. Martinez-Fabregas, J., et al., *CDK8 Fine-Tunes IL-6 Transcriptional Activities by Limiting STAT3 Resident Time at the Gene Loci.* Cell Reports, 2020. **33**(12): p. 108545-108545.
35. Rzymski, T., et al., *SEL120-34A is a novel CDK8 inhibitor active in AML cells with high levels of serine phosphorylation of STAT1 and STAT5 transactivation domains.* Oncotarget, 2017. **8**(20): p. 33779-33779.
36. Yamamoto, S., et al., *Mediator cyclin-dependent kinases upregulate transcription of inflammatory genes in cooperation with NF-κB and C/EBPβ on stimulation of Toll-like receptor 9.* Genes to Cells, 2017. **22**(3): p. 265-276.
37. Shen, S., et al., *rMATS: Robust and flexible detection of differential alternative splicing from replicate RNA-Seq data.* Proceedings of the National Academy of Sciences of the United States of America, 2014. **111**(51): p. E5593-E5601.
38. Obeng, E.A., et al., *Physiologic expression of SF3B1K700E causes impaired erythropoiesis, aberrant splicing, and sensitivity to pharmacologic spliceosome modulation.* Cancer cell, 2016. **30**(3): p. 404-404.
39. Sarchi, M., et al., *Mis-splicing of Mitotic Regulators Sensitizes SF3B1-Mutated Human HSCs to CHK1 Inhibition.* Blood cancer discovery, 2024. **5**(5): p. 353-370.
40. Ashburner, M., et al., *Gene Ontology: tool for the unification of biology.* Nature genetics, 2000. **25**(1): p. 25-25.

41. Consortium, T.G.O., et al., *The Gene Ontology knowledgebase in 2023.* Genetics, 2023. **224**(1).
42. Love, M.I., W. Huber, and S. Anders, *Moderated estimation of fold change and dispersion for RNA-seq data with DESeq2.* Genome Biology, 2014. **15**(12): p. 1-21.
43. Dolatshad, H., et al., *Disruption of SF3B1 results in deregulated expression and splicing of key genes and pathways in myelodysplastic syndrome hematopoietic stem and progenitor cells.* Leukemia 2015 29:5, 2014. **29**(5): p. 1092-1103.
44. Zhang, J., et al., *Disease-Causing Mutations in SF3B1 Alter Splicing by Disrupting Interaction with SUGP1.* Molecular Cell, 2019. **76**: p. 82-95.e7.
45. Pollyea, D.A., et al., *MDS-associated SF3B1 mutations enhance proinflammatory gene expression in patient blast cells.* Journal of Leukocyte Biology, 2020: p. JLB.6AB0520-318RR.
46. Robinson, J.T., et al., *Integrative Genomics Viewer.* Nature biotechnology, 2011 Jan. **29**(1).
47. Banerjee, T., et al., *Flaming and fanning: The Spectrum of inflammatory influences in myelodysplastic syndromes.* Blood reviews, 2019. **36**: p. 57-57.
48. Moura, P.L., et al., *Erythroid Differentiation Enhances RNA Mis-Splicing in SF3B1-Mutant Myelodysplastic Syndromes with Ring Sideroblasts.* Cancer Research, 2024/01/15. **84**(2).
49. Kuppers, D.A., et al., *Gene knock-outs in human CD34+ hematopoietic stem and progenitor cells and in the human immune system of mice.* PloS one, 2023. **18**(6).
50. Chen, K., et al., *Resolving the distinct stages in erythroid differentiation based on dynamic changes in membrane protein expression during erythropoiesis.* Proceedings of the National Academy of Sciences of the United States of America, 2009 Sep 28. **106**(41).
51. HQ, D., et al., *Coexpression of CD71 and CD117 Identifies an Early Unipotent Neutrophil Progenitor Population in Human Bone Marrow - PubMed.* Immunity, 08/18/2020. **53**(2).
52. Hsu, J., et al., *Reprogramming identifies functionally distinct stages of clonal evolution in myelodysplastic syndromes.* Blood, 2019/07/11. **134**(2).
53. Alsafadi, S., et al., *Cancer-associated SF3B1 mutations affect alternative splicing by promoting alternative branchpoint usage.* Nature Communications, 2016. **7**.
54. Dolatshad, H., et al., *Cryptic splicing events in the iron transporter ABCB7 and other key target genes in SF3B1-mutant myelodysplastic syndromes.* Leukemia 2016 30:12, 2016-05-23. **30**(12).
55. Pellagatti, A., et al., *Impact of spliceosome mutations on RNA splicing in myelodysplasia: dysregulated genes/pathways and clinical associations.* Blood, 2018. **132**(12): p. 1225-1240.
56. AK, K., et al., *Cancer-associated SF3B1 mutants recognize otherwise inaccessible cryptic 3′ splice sites within RNA secondary structures - PubMed.* Oncogene, 02/23/2017. **36**(8).
57. MJ, W., et al., *Maintenance of hematopoietic stem cells by tyrosine-unphosphorylated STAT5 and JAK inhibition - PubMed.* Blood advances, 01/28/2025. **9**(2).
58. Johnson, C.S., et al., *Adaptation to ex vivo culture reduces human hematopoietic stem cell activity independently of the cell cycle.* Blood, 2024/08/15. **144**(7).
59. Ng, A.P., *Hit the road JAK, don't P-STAT, stem more!* Blood, 2024/08/15. **144**(7).
60. Fasouli, E.S. and E. Katsantoni, *Frontiers | JAK-STAT in Early Hematopoiesis and Leukemia.* Frontiers in Cell and Developmental Biology, 2021/05/14. **9**.
61. A, W., et al., *c-Myc controls the balance between hematopoietic stem cell self-renewal and differentiation - PubMed.* Genes & development, 11/15/2004. **18**(22).
62. Rodríguez, A., et al., *MYC Promotes Bone Marrow Stem Cell Dysfunction in Fanconi Anemia.* Cell Stem Cell, 2021/01/07. **28**(1).
63. Laurenti, E., et al., *Hematopoietic Stem Cell Function and Survival Depend on c-Myc and N-Myc Activity.* Cell stem cell, 2008 Dec 4. **3**(6).

64. Clough, C.A., et al., *Coordinated missplicing of TMEM14C and ABCB7 causes ring sideroblast formation in SF3B1-mutant myelodysplastic syndrome.* Blood, 2022/03/31. **139**(13).
65. Kuppers, D.A., et al., *Gene knock-outs in human CD34+ hematopoietic stem and progenitor cells and in the human immune system of mice.* PLOS ONE, Jun 28, 2023. **18**(6).
66. HY, L., et al., *PPAR-α and glucocorticoid receptor synergize to promote erythroid progenitor self-renewal - PubMed.* Nature, 06/25/2015. **522**(7557).
67. A, D., et al., *STAR: ultrafast universal RNA-seq aligner - PubMed.* Bioinformatics (Oxford, England), 01/01/2013. **29**(1).
68. Ritchie, M.E., et al., *limma powers differential expression analyses for RNA-sequencing and microarray studies.* Nucleic Acids Research, 2015/04/20. **43**(7).
69. Love, M.I., et al., *Moderated estimation of fold change and dispersion for RNA-seq data with DESeq2.* Genome Biology 2014 15:12, 2014-12-05. **15**(12).
70. Wang, Y., et al., *rMATS-turbo: an efficient and flexible computational tool for alternative splicing analysis of large-scale RNA-seq data.* Nature Protocols 2024 19:4, 2024-02-23. **19**(4).
71. Clement, K., et al., *CRISPResso2 provides accurate and rapid genome editing sequence analysis.* Nature Biotechnology 2019 37:3, 2019-02-26. **37**(3).
72. Chen, E.Y., et al., *Enrichr: interactive and collaborative HTML5 gene list enrichment analysis tool.* BMC Bioinformatics 2013 14:1, 2013-04-15. **14**(1).

Figure Legends

Figure 1. RNA sequencing reveals CDK8 deregulation in Sf3B1 mutant MDS patient samples and isogenic cell lines. (A) Unsupervised clustering (columns) of significant (compared to WT MDS and healthy controls) mis-spliced transcriptional cofactors (read count > 10, |PSI| > 0.08, FDR < 0.05, rows) from publicly available *SF3B1*-mutant MDS patient RNA sequencing data and isogenic cell lines (K562, HNT34). **(B)** Lollipop plot of the Log_2 fold change (DESeq2) of significantly mis-spliced transcriptional co-factors. Yellow, adjusted pvalue < 0.05, blue, adjusted pvalue ≥ 0.05. **(C)** Normalized read counts (DESeq2) of CDK8 mRNA from publicly available data. Dashed line = mean read count of *SF3B1* WT samples. **(D)** IGV plots of the mis-spliced region of CDK8 in *SF3B1* WT and *SF3B1*-mutant MDS patient samples and cell lines. Y-axis, absolute read count. **(E)** RT-PCR and native PAGE of 158 bp surrounding the alternative 3' splice site usage in CDK8 mRNA collected from wildtype and *SF3B1*-mutant cell lines (right). **(F)** Western blot of CDK8 protein levels from wild type and SF3B1 mutant cell lines **(G)** qPCR mean ± SD of isogenic K562 cell lines treated with NMDI-14 (n=3). Treated sample were normalized to untreated controls. *, p < 0.05, 2-way Anova.

Figure 2. Loss of CDK8 alters human HSPC differentiation. (A) Representative flow plots (top) and mean ± SD (bottom) of $CD13^+CD14^+$ myelo-monocytic cells produced by GCSF-mobilized $CD34^+$ cells electroporated with AAVS1 or CDK8 guide RNAs. **(B)** Representative flow plots (top) and mean ± SD (bottom) of $CD71^+$CD235a+ erythroid cells produced by GCSF-mobilized $CD34^+$ cells electroporated with AAVS1 or CDK8 guide RNAs. Data in (A, B) are normalized to non-targeting control (AAVS1). **(C)** Number of colony forming units (CFU) and the types of colonies produced (G/M, granulocyte/macrophage progenitors, BFU-E, burst-forming unit – erythroid). Data are represented as CFU number per 100 plated $CD34^+$ UCB cells electroporated with AAVS1

or CDK8 guide RNAs. **(D)** Representative image of CFU colony pellet following collection at assay termination. *, $p < 0.05$, unpaired two-tailed student's t-test. **(E)** Percentage of human CD45+CD33+CD14+CD16+ intermediate monocytes in the bone marrow of mice (mean ± SD). **(F)** Viable cell number of lineage negative $CD34^+CD38^+$ cells in the bone marrow. **(G)** Percentage lineage negative CD34+CD38- cells in bone marrow (mean ± SD). **(H)** Percentage $Lin^-CD34^+CD38^-$ of hematopoietic stem cells (HSC, $CD90^+CD45RA^-$), multipotent progenitors (MPP, $CD90^-CD45RA^-$), and lymphoid myeloid primmed progenitors (LMPP, $CD90^-CD45RA^+$) cells in bone marrow (mean ± SD). **(I)** Percentage Lin-CD34+CD38+ megakaryocyte erythroid progenitors (MEP, $CD45RA^-CD123^-$), common myeloid progenitors (CMP, $CD45RA^-CD123^+$), and granulocyte macrophage progenitors (GMP, $CD45RA^+CD123^+$) in the bone marrow. **(J)** Viable cell number of $Lin^-CD34^+CD38^+CD71^+$ cells in the bone marrow.

Figure 3. Homeostatic and lineage pathways are deregulated by CDK8 loss. (A) Experimental overview for RNA sequencing experiment. **(B)** Volcano plot representation of differentially expressed genes from CDK8 knock-down cells compared to non-targeting control, showing the magnitude of difference ($\log_2$ fold change, x-axis) and significance ($-\log_{10}$(adjusted p-value), y-axis). Red dots, adjusted p-value < 0.05, LFC >0.5, blue dots, adjusted p-value < 0.05, LFC <0.5, solid dots, significant genes across both shRNAs. Dashed lines mark the cutoff for significance (horizontal, adjusted p-value < 0.05) and fold change (vertical, -0.5 < LFC >0.5). **(C)** Volcano plot representation of differentially expressed genes from *SF3B1*-mutant patient samples compared to *SF3B1*-WT MDs and healthy controls. Dots, genes shown to be significantly up (red) or down (blue) in CDK8 knockdown $CD34^+$ HSPCs, grey circles, all other genes.

Figure 4. CDK8 re-expression rescues early erythroid differentiation. (A) Experimental overview for erythroid differentiation assay using the iPSC-HPC model. **(B)** RT-PCR and native PAGE of 158 bp surrounding the alternative 3' splice site usage in CDK8 mRNA collected from wildtype (WT) and SF3B1 G742D mutant iPSC-HPCs. **(C)** Western blot of CDK8 protein levels from SF3B1 wildtype and mutant iPSC-HPCs. **(D)** Western blot (top) and quantification of iPSC-HPCs transduced with lentiviral particles containing empty vector (EV), or full length CDK8 wildtype (CDK8 WT) cDNA. Western blot was quantified and protein ratio (relative to loading control, ImageJ) was plotted (bottom). **(E)** Representative flow plots and **(G)** mean ± SD (bottom) of $CD71^{+}CD235a^{+}$ iPSC-HPCs transduced with CDK8 WT cDNA or EV control on day 4 of erythroid differentiation. **(F)** Representative flow plots and **(H)** mean ± SD (bottom) of CD71+CD235a+ iPSC-HPCs transduced with CDK8 WT cDNA or EV control on day 13 of erythroid differentiation. *, $p < 0.05$, **, $p < 0.01$, ***, $p< 0.001$, ****, $p < 0.0001$ ordinary one-way Anova.

Figures

Figure 1

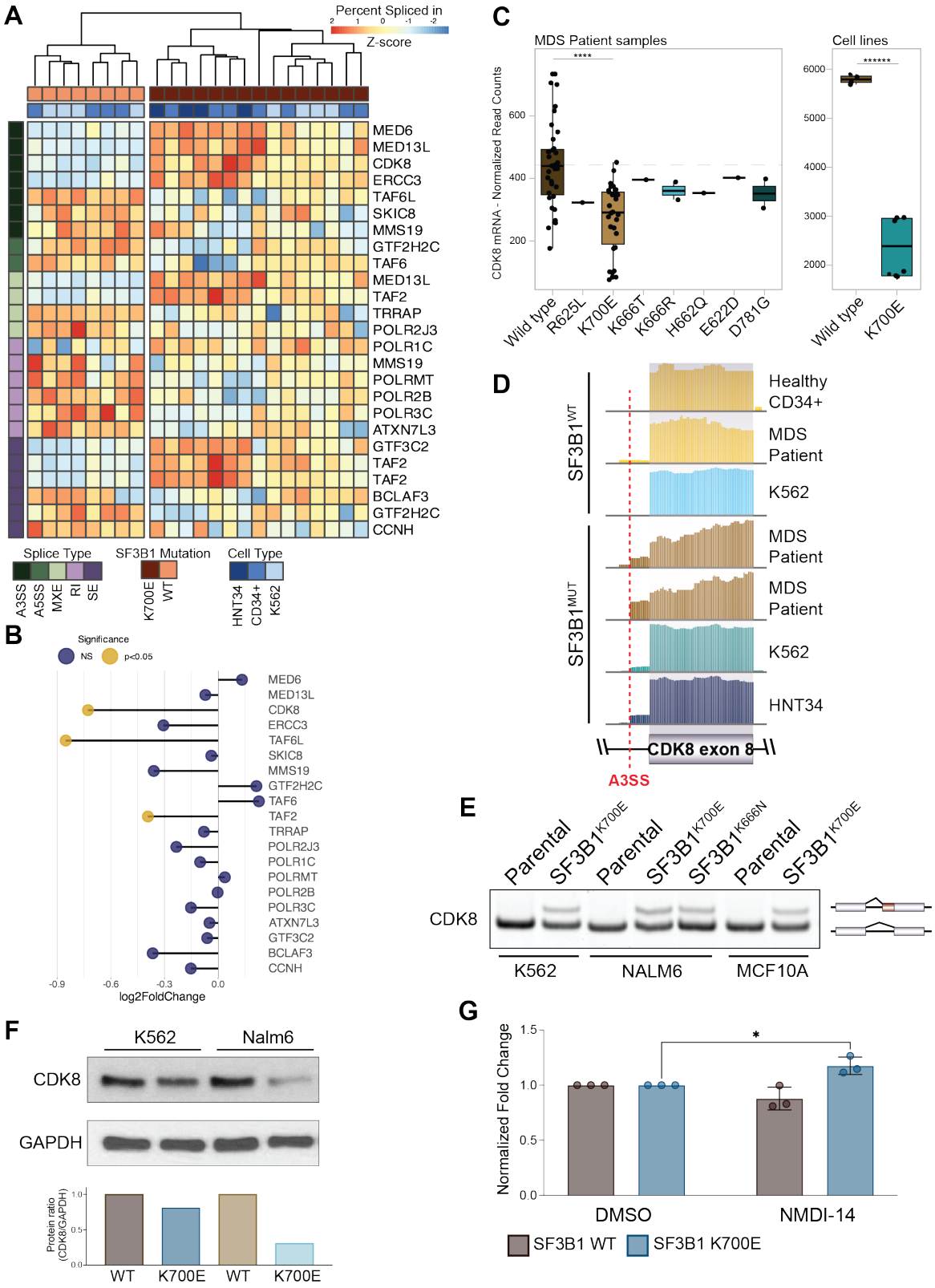

Figure 2

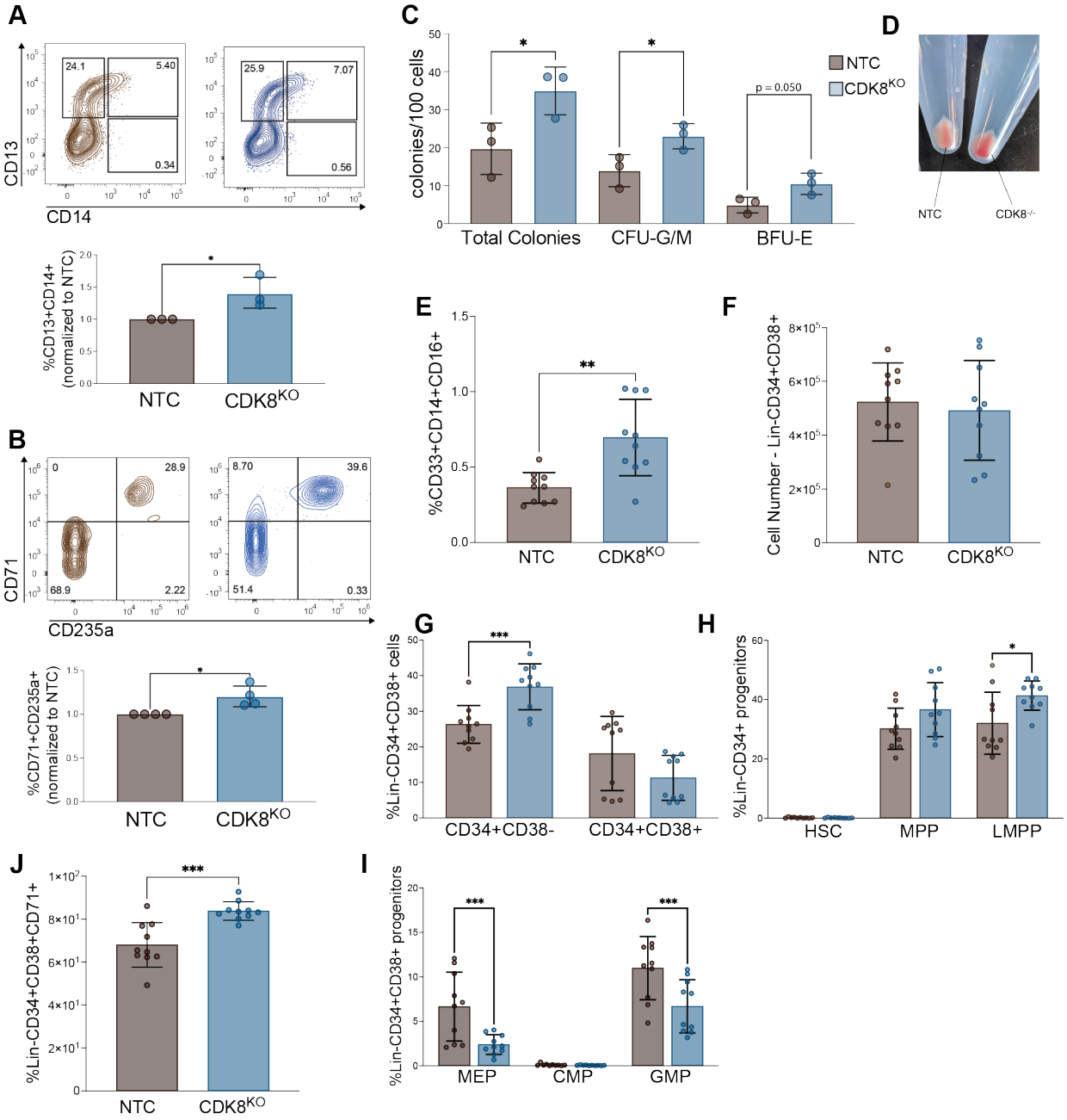
A
CD13
CD14
24.1
5.40
0.34
25.9
7.07
0.56
%CD13+CD14+ (normalized to NTC)
NTC
CDK8KO
B
CD71
CD235a
0
28.9
68.9
2.22
8.70
39.6
51.4
0.33
%CD71+CD235a+ (normalized to NTC)
NTC
CDK8KO
C
colonies/100 cells
Total Colonies
CFU-G/M
BFU-E
p = 0.050
NTC
CDK8KO
D
NTC
CDK8-/-
E
%CD33+CD14+CD16+
NTC
CDK8KO
F
Cell Number - Lin-CD34+CD38+
NTC
CDK8KO
G
%Lin-CD34+CD38+ cells
CD34+CD38-
CD34+CD38+
H
%Lin-CD34+ progenitors
HSC
MPP
LMPP
J
%Lin-CD34+CD38+CD71+
NTC
CDK8KO
I
%Lin-CD34+CD38+ progenitors
MEP
CMP
GMP

Figure 3

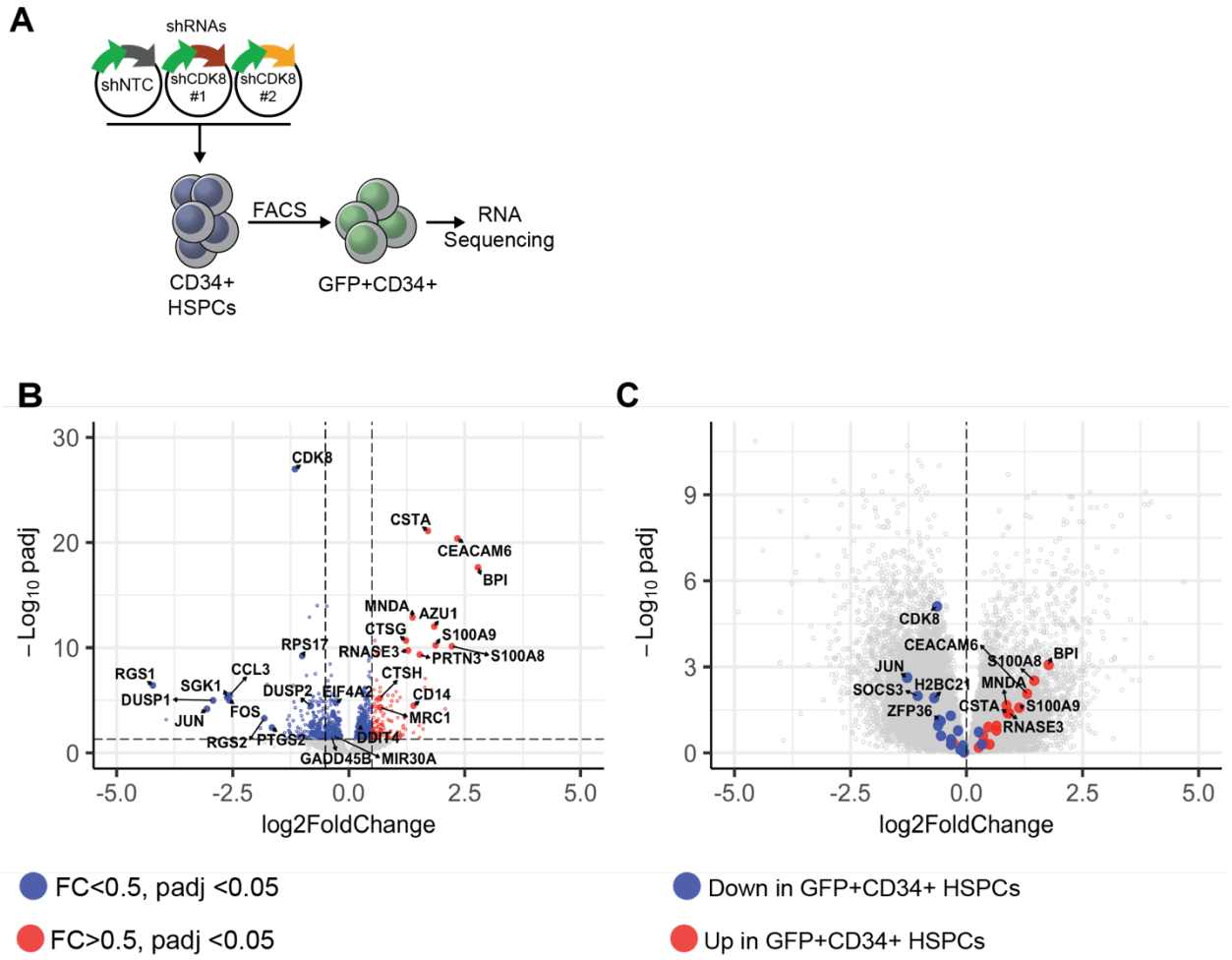
A
shRNAs
shNTC
shCDK8 #1
shCDK8 #2
FACS
RNA Sequencing
CD34+ HSPCs
GFP+CD34+
B
C
– Log10 padj
log2FoldChange
CDK8
CSTA
CEACAM6
BPI
MNDA
AZU1
CTSG
S100A9
RNASE3
PRTN3
S100A8
RPS17
CTSH
CD14
MRC1
DDIT4
MIR30A
GADD45B
RGS1
SGK1
CCL3
DUSP1
DUSP2
EIF4A2
FOS
JUN
RGS2
PTGS2
JUN
SOCS3
H2BC21
ZFP36
FC<0.5, padj <0.05
FC>0.5, padj <0.05
Down in GFP+CD34+ HSPCs
Up in GFP+CD34+ HSPCs

Figure 4

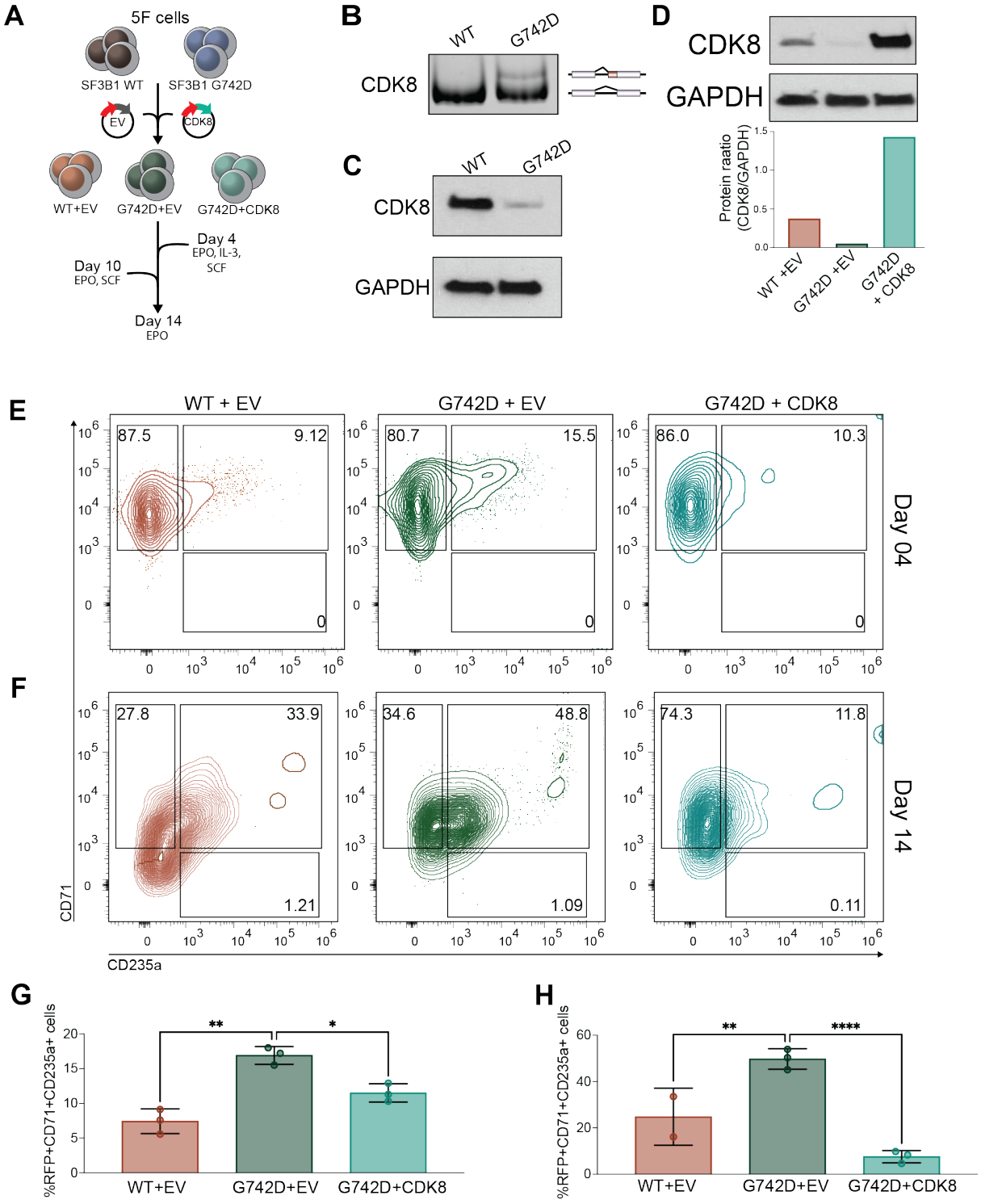
A
5F cells
SF3B1 WT
SF3B1 G742D
EV
CDK8
WT+EV
G742D+EV
G742D+CDK8
Day 4
EPO, IL-3, SCF
Day 10
EPO, SCF
Day 14
EPO
B
WT
G742D
CDK8
C
WT
G742D
CDK8
GAPDH
D
CDK8
GAPDH
Protein raatio (CDK8/GAPDH)
WT +EV
G742D +EV
G742D + CDK8
E
WT + EV
G742D + EV
G742D + CDK8
87.5
9.12
0
80.7
15.5
0
86.0
10.3
0
Day 04
F
27.8
33.9
1.21
34.6
48.8
1.09
74.3
11.8
0.11
Day 14
CD71
CD235a
G
%RFP+CD71+CD235a+ cells
**
*
WT+EV
G742D+EV
G742D+CDK8
H
%RFP+CD71+CD235a+ cells
**
****
WT+EV
G742D+EV
G742D+CDK8